JPE 17-4-12

https://doi.org/10.6113/JPE.2017.17.4.963
ISSN(Print): 1598-2092 / ISSN(Online): 2093-4718

Acoustic Noise of Brushless DC Motors Induced by Electromagnetic Torque Ripple

Kun Xia†, Zhengrong Li*, Jing Lu*, Bin Dong*, and Chao Bi*

†,*Department of Electrical Engineering, University of Shanghai for Science and Technology, Shanghai, China

Abstract

Torque ripple is one of the major sources inducing vibration and noise in brushless DC motors. This is especially true in applications such as the spindle motors used in hard disk drives. However, the relationship between torque ripple and acoustic noise/vibration is quite complicated. This paper presents a way to investigate this relationship with acoustic noise measurement and analysis. Results obtained with three different drive modes are used in the analysis. The results show that the acoustic noise analysis is very helpful in designing a high-performance drive strategy for BLDC motors.

Key words: Acoustic noise, BLDC motor, Drive strategy, Torque ripple

I. INTRODUCTION

Brushless DC (BLDC) motors make themselves attractive in industrial applications owing to their many advantages. However, torque ripple is one of the worst drawbacks that results in mechanical vibration and acoustic noise [1].

Acoustic noise sources may be categorized into mechanical and electromagnetic (EM) noises for BLDC motors. The mechanical noises include the noises caused by the windage friction of the rotor surface and the rolling of bearing balls rotating at high speeds; while the EM noises are formed by unbalanced magnetic pull (UMP) [2]-[6] and torque ripples [7], [8]. Acoustic noise resulting from the motor deformation induced by the radial magnetic field, may also be considered as EM noise [9].

UMP is determined by the EM structure of the motor, the quality of the components, and the quality of the motor assemblage. The noise from UMP may be reduced to a minimal value with a fine motor design and precise production technology [10]. Moreover, for BLDC motors with no less than four magnetic pole-pairs, the deformations of tested motors caused by the drive current can be neglected [11].

Torque ripples in a BLDC motor consist of cogging torque and operation torque ripples. Cogging torque ripple is a common defect in permanent magnet motors, and it can be minimized via a better motor design [12]. Operation torque ripple can be classified into commutation torque ripple and inherent torque ripple. The former occurs in the current commutation interval, and later is present in the steady conduction state. Methods for commutation torque-ripple reduction have been reported in [13], [14]. The effects of a non-ideal back-EMF waveform and a reduction method for inherent torque ripple have been discussed in [15].

However, the direct measurement of torque ripple is very difficult for miniature and high speed motors, like the spindle motors used in hard disk drives (HDD). The torque estimation method that is primarily used in direct toque control (DTC) [16] is difficult to use when the parameters of the motor keep changing during rotation. In practice, a torque sensor is also unfit for use in torque ripple measurement because of its reduced frequency response in high speed regions. Although several new methods to measure torque have been developed in recent years, e.g., fiber grating [17], differential magnetic [18] and surface acoustic wave [19], they are too complicated for practical use.

The EM acoustic noise of a motor induced by EM torque force acquires information on torque ripples, and is suitable for torque ripple detection when miniature BLDC motors operate at high speeds or without a load. At the meantime, there are more studies being done on the EM acoustic noise of BLDC motors and methods to reduce it [6], [24], [25]. The authors of [23] introduced a method for briefly inducing electromagnetic torque ripple by acoustic noise. However, they did not

Manuscript received Dec. 14, 2016; revised Mar. 27, 2017
Recommended for publication by Associate Editor Bon-Gwan Gu.
†Corresponding Author: new_energy@usst.edu.cn
Tel: +86-137-6111-9291, Fax: +86-5527-4148, Univ. Shanghai Sci. Tech.
*Dept. of Electrical Eng., Univ. of Shanghai for Science and Tech., China

provided enough detail nor reference torque data.

This paper will provide a detailed investigation of the influence of EM torque ripple on the acoustic noise of a motor to identify the torque level of the motor. Different torque ripples and acoustic noises in BLDC motors are analyzed. Three driving methods are employed in this study to illustrate the relationship between torque ripple and acoustic noise. For comparison, torque ripples are also measured by a torque transducer. The obtained results indicate that measurements of EM acoustic noise are an effective reflection of EM torque ripple, and are meaningful for BLDC motor design and control.

II. Torque Ripple in BLDC Motors

There are many control strategies for three-phase BLDC driving systems, and the most popular is the six-step square-wave driving method. To simplify the description, the drive mode with constant dc-link voltage is named the constant voltage drive mode (CV-mode) in this paper.

A. Commutation Torque Ripple

The ideal back-EMF waveform shapes of BLDC motors, e_a, e_b, and e_c, are shown in Fig. 1. It can be seen that they have trapezoidal shapes. When the stator windings of phases A, B, and C are fed with square wave currents, the EM torque force T_{em} on the motor shaft is constant and can be expressed as:

$$T_{em} = \left(e_a i_a + e_b i_b + e_c i_c\right)\frac{1}{\omega_r} \tag{1}$$

where ω_r is the mechanical angular speed of the rotor.

In Fig. 1, T_a, T_b, and T_c are the EM torque force of each phase. Ideal back-EMF BLDC motors operating under the CV-mode do not generate EM torque ripple. However, the expected square waveform current is hard to achieve for the inductance of the motor armature winding. The difference between the rising and falling rates of the phase currents directly contributes to commutation torque ripple. Commutation torque ripple can reach 50% of the average output torque when using the traditional BLDC drive mode [12].

The conventional driving system for BLDC motors is shown in Fig. 2. The switching states of the CV-mode are generated by the controller according to the rotor position signals. The PWM_ON scheme, which has the least commutation ripple when compared with other PWM strategies, is applied in this paper. Fig. 3(a) shows the phase current waveforms and the gate signals on the inverter switches in the CV-mode at the commutation interval when the phase current is changing from phase-AB to phase-AC. The current jumping at commutation period contributes to the commutation torque ripple.

Considering that the commutation is very quick, the back-EMF can be processed as a constant during commutation. In the following, only the commutation process of the phase current from phase-AB to phase-AC is analysed. The current of phase B cannot immediately drop to zero at the beginning of the commutation, and it flows through the freewheeling diode of T_3. The stator terminal voltage during the commutation interval can be illustrated as:

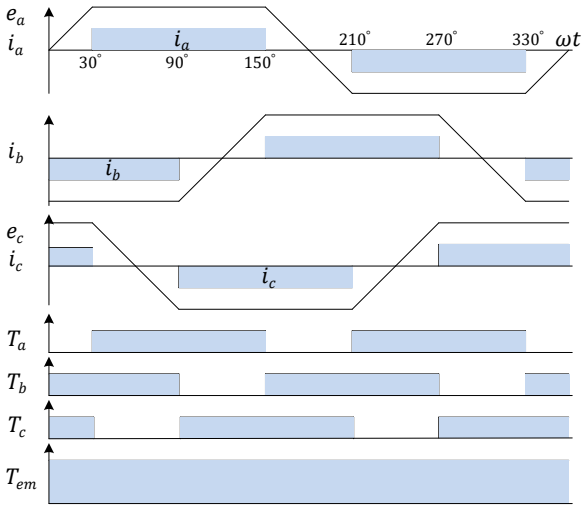

Fig. 1. Ideal back EMF, phase current, and torque waveform of a BLDC motor.

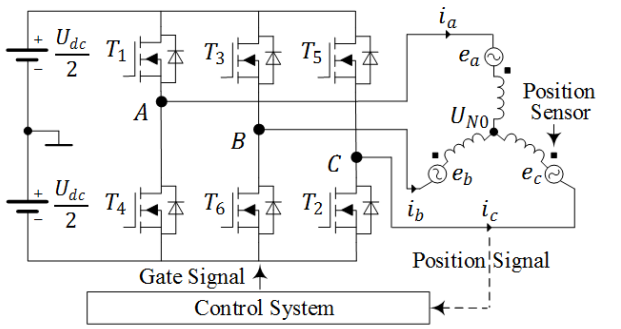

Fig. 2. Conventional driving system of a BLDC motor.

$$\begin{cases} \dfrac{U_{dc}}{2} = Ri_a + L\dfrac{di_a}{dt} + e_a + U_{No} \\ \dfrac{U_{dc}}{2} = Ri_b + L\dfrac{di_b}{dt} + e_b + U_{No} \\ -\dfrac{U_{dc}}{2}(2D-1) = Ri_c + L\dfrac{di_c}{dt} + e_c + U_{No} \end{cases} \tag{2}$$

where U_{dc} is the dc-link voltage, D is the duty ratio of the PWM on the inverter switches, L is the phase equivalent inductance of the stator windings that can be calculated from the self-inductance L_s and mutual inductance M for individual coils as $L = L_s - M$, and R is the stator winding resistance.

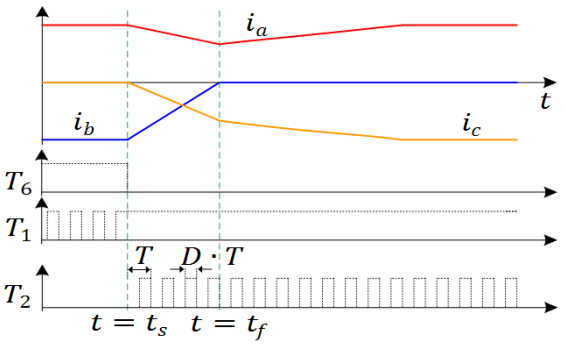

(a) CV-mode.

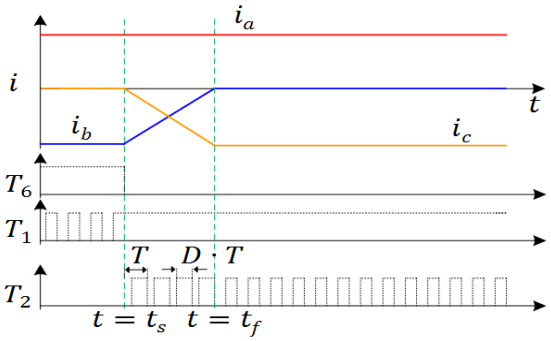

(b) VV-mode.

Fig. 3. Switching patterns with current waveforms.

According to the instantaneous power theory, the voltage of the motor neutral point can be described as:

$$U_{N0} = \left(\frac{3U_{dc}}{2} - DU_{dc} - e_a - e_b - e_c \right) / 3 \tag{3}$$

It is assumed that the phase resistance is relatively small. Neglecting the influence of the resistance, the current derivative of phase-A can be given by:

$$\left(\frac{di_a}{dt} \right)_{ts} = \frac{DU_{dc} - 2e_a + e_b + e_c}{3L} \tag{4}$$

At the beginning of the commutation, the back-EMF of each phase can be expressed as $e_a = E_m$, $e_b = -E_m$, and $e_c = -E_m$, where E_m is the amplitude of the back-EMF. From the torque equation, the rising and falling speeds of the current should be equal to produce a constant output torque during the commutation period, and it always exists as:

$$DU_{dc} = 4E_m \tag{5}$$

which implies that the commutation torque ripple can be suppressed when the duty ratio of the PWM maintains $4E_m / U_{dc}$.

Normally, the value of D in the commutation interval should be larger than the duty ratio in the steady conduction state. When the needed D during commutation is greater than 1 at high speeds ($D > 1$), the voltage boost converter should be applied in front of the inverter [20]. Utilizing this variable-voltage drive mode (VV-mode), the current jumping during commutation can be minimized. Fig. 3(b) shows the phase current waveform and switching pattern of a BLDC motor in the VV-mode.

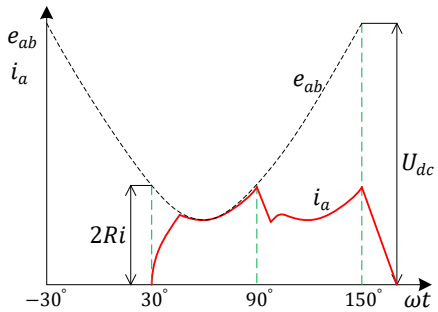

Fig. 4. Phase current under a non-ideal back-EMF.

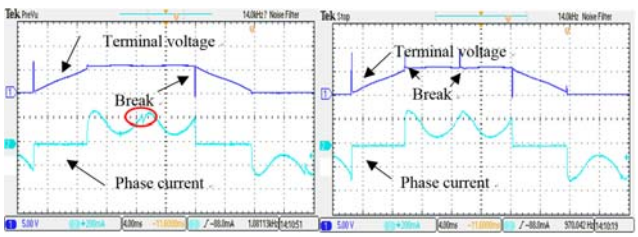

(a) CV-mode. (b) VV-mode.

Fig. 5. Measured waveforms when operating without a load.

B. Inherent Torque Ripple

As shown in Fig. 3(b), there is no torque ripple under the ideal trapezoid back-EMF. However, due to the constraints of motor manufacturing technology, the waveform of the back-EMF in many motors is actually more quasi-sine-wave in shape than trapezoidal. This is caused by the use of concentrated armature winding, e.g., the spindle motors used in HDDs. Due to the non-ideal back-EMF, the current is no longer a square-wave during the conduction state, which leads to an inherent torque ripple. Fig. 4 illustrates the phase current waveform under a non-ideal back EMF in the CV-mode. Where e_{ab} and i_a are the back-EMF of phase A to phase B and the phase A current, respectively.

The break in the terminal voltage at the commutation interval is caused by the free-wheeling diode in the out-going phase. In addition, the peak of the stator terminal voltage is generated by the boost converter in the VV-mode. The current jumping marked with an ellipse in Fig. 5(a) is caused by the BLDC motor commutation. It can be reduced in the VV-mode as shown in Fig. 5(b). The back-EMF waveforms of a motor running without currents in the stator windings are shown in Fig. 6. They resemble a poorly shaped sinusoidal waveform. However, the space vector drive mode (SV-mode) can eliminate both the inherent and commutation torque ripple of permanent magnet motors with a sinusoidal back-EMF waveform [8]. The SV-mode aims at forming a uniform rotating magnetic field with a constant amplitude.

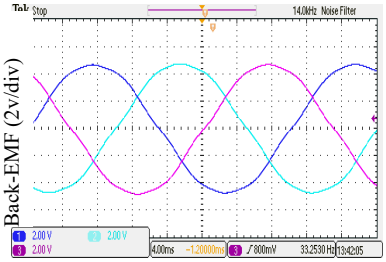

Fig. 6. Measured back-EMF waveform of a BLDC motor.

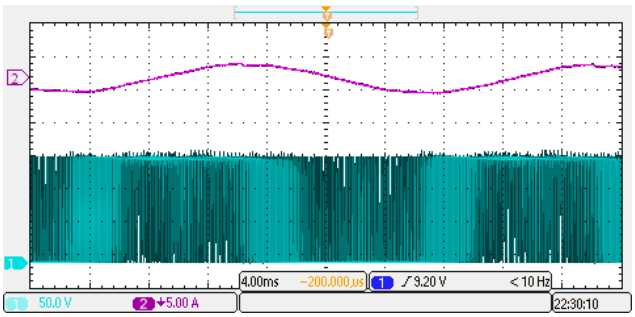

Fig. 7. Current and gate signal waveforms of Q4.

Comparing the 7-step SV-mode and the 5-step SV-mode, the former produces less harmonic and the latter one, which was adopted in this paper, has a lower switching frequency. As shown in Fig.7, channel 1 is the gate signal for the lower arm switch Q4 and channel 2 is the phase current of the motor.

III. Acoustic Noise Source of BLDC Motors

The acoustic noise in BLDC motors includes both EM and mechanical noise. The EM noise in BLDC motors is primarily caused by variations of the EM force/torque acting on the rotor and stator parts, which generate the EM torque to drive the rotor to rotate.

BLDC motors commutate every 60°in one electrical cycle in the CV-mode and VV-mode. The current variation gives rise to EM acoustic noise, and the fundamental frequency of the acoustic noise from the current is the commutation frequency of the BLDC motor [21]. The frequency of the harmonics of the EM acoustic noise should be:

$$f_{i^{th}} = i \times k \times p \times \frac{n}{60} \quad i = 1,2,3... \tag{6}$$

where $f_{i^{th}}$ is the i^{th} order harmonics of the motor commutation frequency, i is the number of the harmonics order, k is the number of steps of commutation in one electrical cycle, p is the number of stator pair of poles, and n is the rotational speed (r/min). In the CV-mode and VV-mode k = 6. Thus, the fundamental commutation frequency $f_{1^{th}}$ is $0.1pn$.

The fundamental frequency of mechanical noise is:

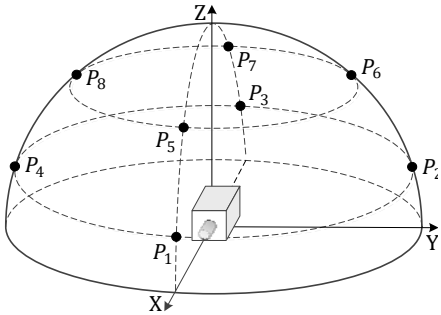

Fig. 8. Selected points for measuring the SPL of a BLDC motor.

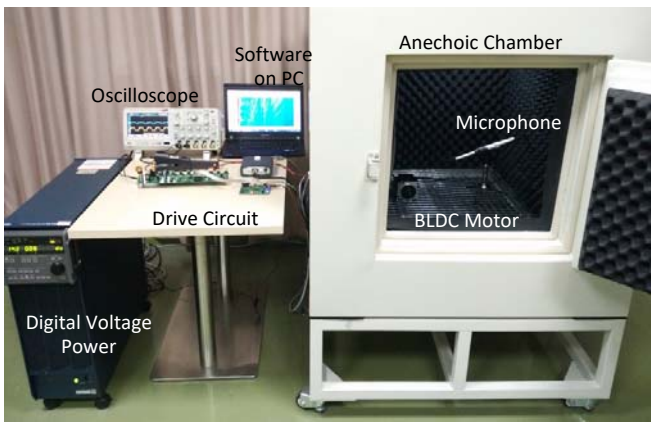

Fig. 9. Experimental system for acoustic noise measurement.

$$f_s = \frac{n}{60} \tag{7}$$

BLDC motor systems resonate as the frequencies of the excitation force components move closer to any of their axial resonant frequencies [22]. Resonant frequency is inherent in a motor and determined by the motor structure and by the materials used. Considering the motor as an elastic system, the resonant frequency can be expressed as:

$$f_c = \frac{1}{2\pi}\sqrt{k_s / m} \tag{8}$$

where k_s is the stiffness and m is the mass of the elastic system.

The fundamental resonant frequency of the stator can be calculated as:

$$f_{c0} = \frac{1}{2\pi}\sqrt{\frac{Eh_j}{m'R_j^2}} \tag{9}$$

where h_j and R_j are the radial height and average radius of the stator yoke, respectively. m' is the surface mass on the average radius of the stator yoke, and E is the elastic modulus.

Acoustic noise is obtained through the sound pressure level meter and it is recorded by the measurement system. Thus, the spectrum of the sound pressure level (SPL) can be obtained in post processing. To precisely measure the

TABLE I
PARAMETERS OF A BLDC MOTOR.

Parameters	Value
Rated Voltage (V)	36
Rated Power (W)	200
Rated Speed (r/min)	2000
Rated Torque (N.m)	0.8
Pole Pairs	5
Phase Resistance (Ω)	0.2
Phase Inductance(μH)	395.3

acoustic noise, the sound pressures at points P_1 to P_8 are measured step by step in an anechoic chamber. The eight points surrounding the tested motor are shown in Fig. 8. Each test points is 20 cm from the motor. From the SPL of the eight selected test points, the average SPL of the tested motor at a distance of 20 cm can be calculated as:

$$\overline{L_p} = 10\log\left\{\frac{1}{N}\left(\sum_{i=1}^{N} 10^{\frac{L_{p,i}}{10}}\right)\right\} \tag{10}$$

where $\overline{L_p}$ is the average SPL of the tested BLDC motor. $L_{p,i}$ and N denote the SPL at each point and the number of measurement points, respectively.

The acoustic noise testing system is shown in Fig. 9. Due to the limited space in the chamber, only one microphone is used in the one-time test. The whole test is formed by 8 tests step by step, where the microphone is placed in different locations. These positions are the positions P_1 to P_8 shown in Fig. 8. The SPL spectrum of the background noise of the chamber is shown in Fig. 10(a).

IV. EXPERIMENTAL RESULTS

Several motors were operated to investigate the roots of the acoustic noise. In this section, three different drive-mode experiments on BLDC motors with a ball bearing are shown and discussed. Firstly, the SPL spectrums of BLDC motors obtained by the proposed method are demonstrated and analysed. Secondly, statistics for the BLDC motors gathered by a torque transducer are investigated. The results show that acoustic noise is substantially helpful for the torque ripple analysis of BLDC motors. They determine that changing the drive mode affects the acoustic noise for this kind of motor. The key parameters for the motor are listed in Table I.

The frequency of the PWM is 30 kHz, which is above the audible range to prevent the introduction of external interference.

The acoustic noise of BLDC motors is affected by both the commutation and inherent torque ripple in the CV-mode. The SPL spectrum of the test point P_2 for the tested motor is shown in Fig. 10(b). The range of the SPL spectra is from 0

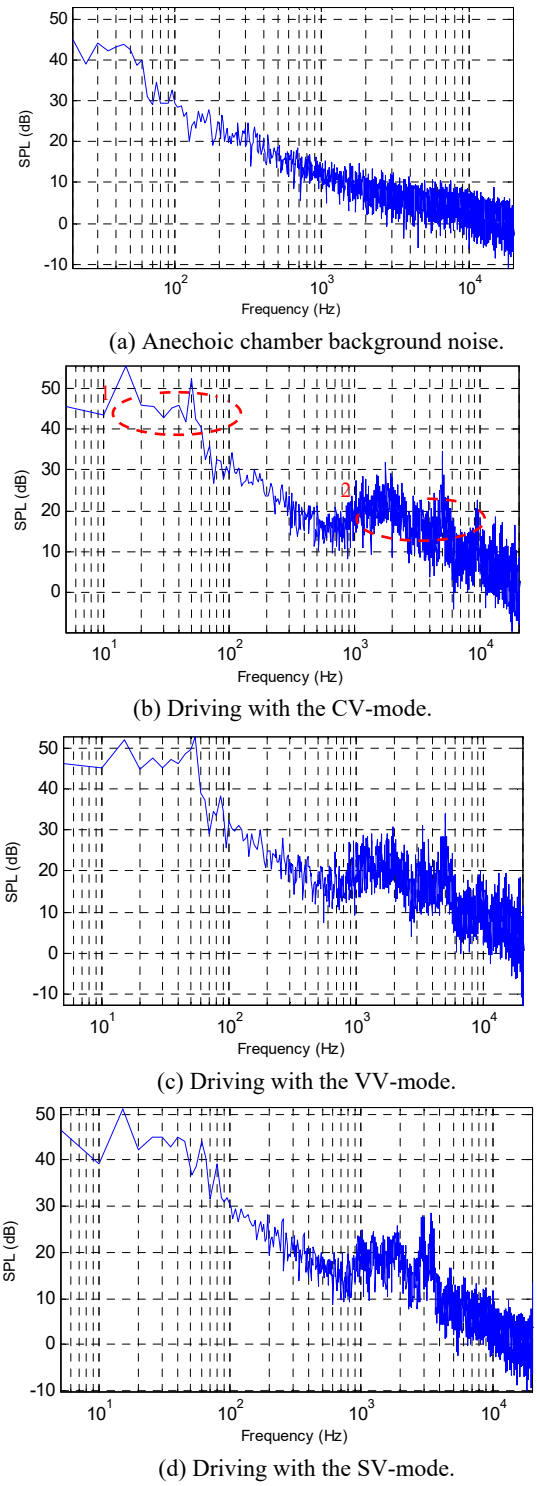

(a) Anechoic chamber background noise.

(b) Driving with the CV-mode.

(c) Driving with the VV-mode.

(d) Driving with the SV-mode.

Fig. 10. SPL spectrum for a BLDC motor.

to 20 kHz. The meaningful testing data, compared with the background noise SPL spectrum, is marked with two ellipses in Fig. 10(b).

The rotating speed is 1000 r/min and the fundamental frequency of the commutation f_1^{th} is 500 Hz in the CV-mode and the VV-mode. Mechanical noise in the low

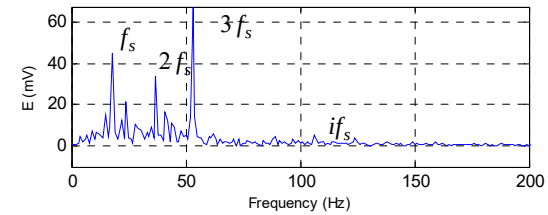

(a) Mechanical noise.

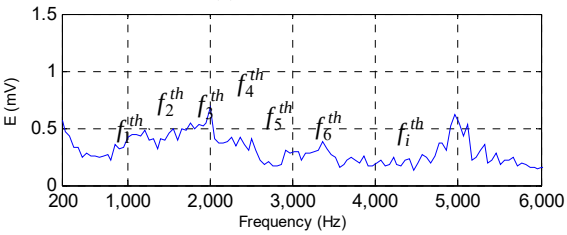

(b) EM noise.

Fig. 11. Sound amplitude spectra.

TABLE II
MEASURED SPL FOR EACH POINT-NOISE (DB)

Point	CV-mode	VV-mode	SV-mode
P_1	52.4	51.6	45.2
P_2	53.8	53.4	47.9
P_3	53.4	53.7	46.0
P_4	54.7	53.8	46.2
P_5	46.8	46.6	45.2
P_6	47.4	46.7	42.0
P_7	48.7	47.3	47.0
P_8	45.5	44.9	41.2
$\overline{L_p}$	51.54	51.03	45.57

frequency range extends from the fundamental frequency 18 Hz to the quintuple frequency 90 Hz, as marked with the first ellipse in Fig. 10(b). The second ellipse shows the EM noise of the BLDC motor from f_1^{th} to f_{11}^{th}, which is in the high frequency range from 500 to 6000 Hz. The corresponding sound amplitudes of the two ellipses are also shown in Fig. 11, where the value of the sound spectrum is given in mV. The sound pressure level can be calculated from the sound amplitude.

Using the VV-mode, the current jumping in the commutation interval can be reduced. Thus, the commutation torque ripple can be effectively suppressed. However, this is still a "six-step" drive mode, and the inherent torque ripple should not change. The SPL spectrum on point P2 in the VV-mode is shown in Fig. 10(c).

The SV-mode, which has been used in many applications of PM motor driving, can significantly reduce the commutation current jumping. This drive mode can also noticeably reduce the inherent torque ripple. Therefore, the acoustic noise induced by the drive mode should be the lowest. The SPL spectrum in the SV-mode of the P2 measuring point is shown in Fig. 10(d).

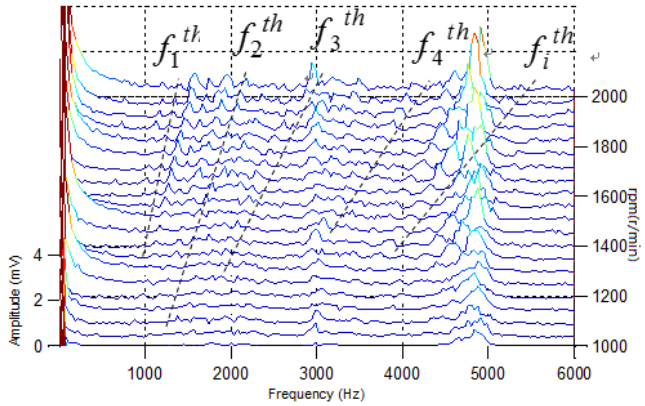

(a) Driving with the CV-mode.

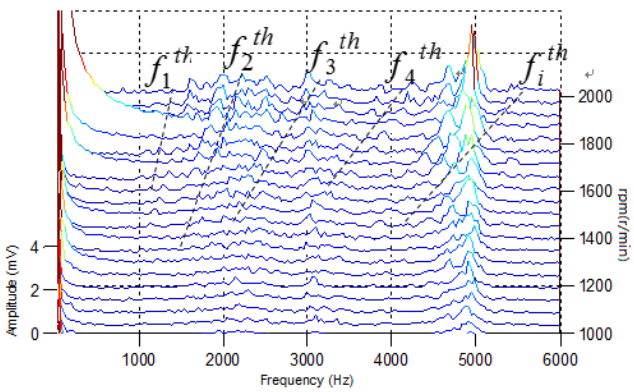

(b) Driving with the VV-mode.

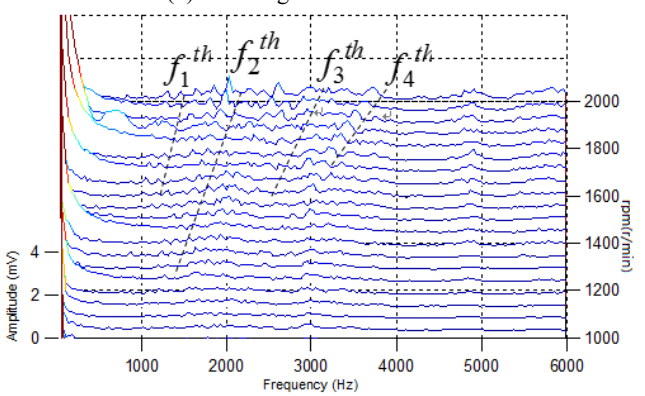

(c) Driving with the SV-mode.

Fig. 12. Acoustic noise spectra waterfalls.

The SPL value of each point is shown in Table II. The average SPL of the tested motor in the SV-mode is 45.57 dB, which is much lower when compared with the noise in the CV-mode and VV-mode. This clearly shows the influence the torque ripple has on the acoustic noise.

From TABLE II, it can be seen that the VV-mode can reduce the acoustic noise at all of the measuring points from P_1 to P_8. Comparing Fig. 10(b) with Fig. 10(c) shows that the VV-mode can also slightly reduce the noise. Considering that, the inherent torque ripple of the CV-mode is almost the same as the VV mode, and the spectrum of the commutation

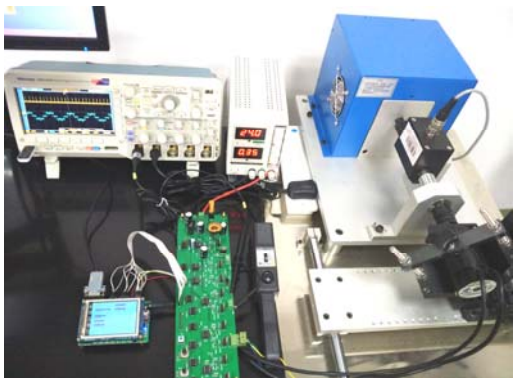

Fig. 13. BLDCM torque measurement system.

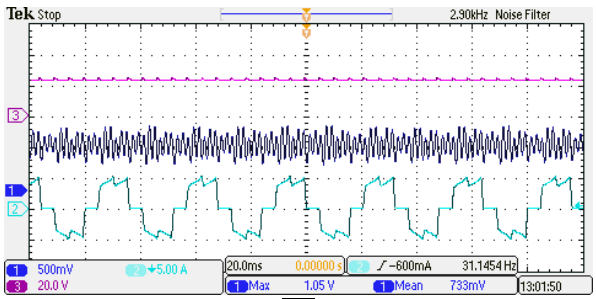

(a) Driving with the CV-mode.

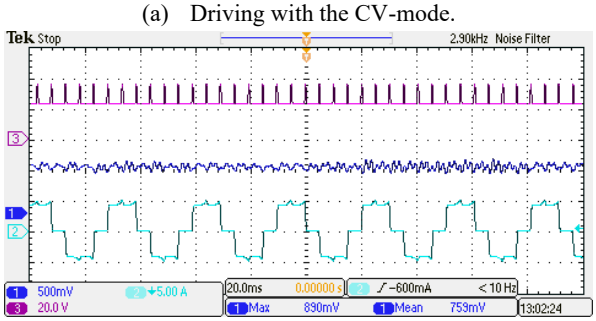

(b) Driving with the VV-mode.

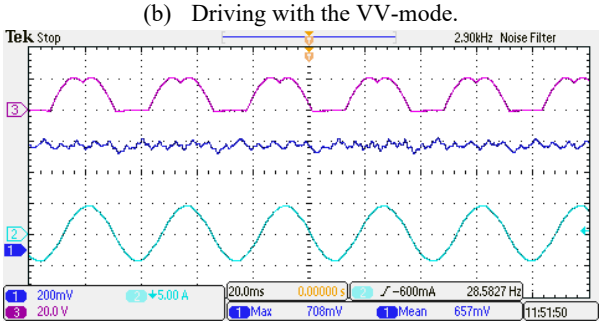

(c) Driving with the SV-mode.

Fig. 14. Experiment waveforms of a BLDCM.

current jumping is very wide, i.e., the included this, the commutation torque ripple is the major source of the EM acoustic noise of BLDC motors. This conclusion can also be confirmed from the SV-mode experimental results, where the commutation current jumping is reduced to its minimum, and its acoustic noise is the lowest in the three drive modes.

The torque transducer can be used to measure the output torque of a BLDCM with a load. Fig.13 show the structure of the test system. Experimental waveforms when the BLDCM operates with a load are shown in Fig.14. The first channel is the output torque ripple measured with the torque transducer. The second channel is the phase current. The third channel in Fig.14 (a) and (b) are the DC-link voltages of the driving circuit, while Fig.14 (c) it is the reference voltage waveform for the SVPWM. The results show that the SV-mode driving method can achieve a minimum torque ripple.

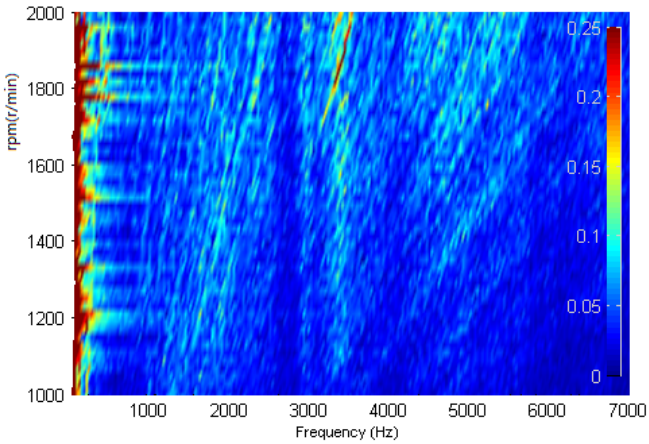

Fig. 15. Waterfall of the EM acoustic noise amplitudes.

The waterfall processing of acoustic noise is widely used in the mechanical system analyses. The waterfall format of the motor acoustic noise driven by the CV-mode, the VV-mode and the SV-mode are shown in Fig. 12 for the ranges of the ellipses shown in Fig. 10(b). It is known that the torque ripple in the SV-mode is the minimum, while that in the CV-mode is the maximum among the three drive modes. The amplitude of the commutation frequency points marked with dotted lines in each of the subfigures of Fig. 12 is proportional to the torque ripple in the different drive modes. Therefore, it can be clearly judged that the VV-mode is better than the traditional CV-mode in the reduction of acoustic noise. The SV-mode is the best among the three modes.

The amplitudes of the acoustic noise are much higher at approximately 3000 Hz for all of the rotating speeds in Fig. 15. This is the resonant frequency where the acoustic noise cannot be eliminated with the changing drive mode. It is clear that the resonance frequency is only determined by the motor structure, the assembling process, and the material used. From the experimental figures, it can be concluded that using the SV-mode, the noise at the resonance point is the weakest in all three modes since the exciting source of the resonance, i.e., the torque ripple, is the weakest for the SV-mode.

V. CONCLUSIONS

Judging the effectiveness of the drive mode in torque ripple reduction is difficult, especially when it comes to miniature and high speed motors, like the spindle motors used in HDDs. The results presented in this paper show that the

acoustic noise test and waterfall processing can clearly identify the sources of EM acoustic noise in BLDC motor operation. Thus, they can be used to identify the generation of torque ripple in motor operation. From the results of the Constant-Voltage drive mode, the Variable-Voltage drive mode and the Space-Vector drive mode, it can be found that measurements of the EM acoustic noise are a very effective reflection of EM torque ripple detection, and that the SV-mode can supress EM acoustic noise better than the traditional VV-mode and CV-mode. This is a lot more convenient for detecting EM torque ripple than the traditional methods when it comes to developing a high performance motor drive mode for the applications like the spindle motor control of HDDs, where the acoustic noise/vibration must be low and speed control must be robust. The acoustic noise test and waterfall processing can also help researchers in improving motor structure since the mechanical roots of the acoustic noise can also be clearly identified.

ACKNOWLEDGMENT

This work was supported in part by the National Natural Science Foundation of China, under grant No. 51207091.

REFERENCES

[1] S. A. Saied and K. Abbaszadeh, "Cogging torque reduction in brushless DC motors using slot-opening shift," *Advances in Electrical & Computer Engineering,* Vol. 9, No. 1, pp. 28-33, Feb. 2009.

[2] D. M. Ionel, M. Popescu, M. I. McGilp, T. J. E. Miller, and S. J. Dellinger, "Assessment of torque components in brushless permanent-magnet machines through numerical analysis of the electromagnetic field," *IEEE Trans. Ind. Appl.,* Vol. 41, No. 5, pp. 1149-1158, Sep./Oct. 2005.

[3] J. Y. Song, K. J. Kang, and C. H. Kang, and G. H. Jang, "Cogging torque and unbalanced magnetic pull due to simultaneous existence of dynamic and static eccentricities and uneven magnetization in permanent magnet motors," *IEEE Trans. Magn.,* Vol. 53, No. 3, Mar. 2017.

[4] J. Le Besnerais, Q. Souron, and E. Devillers, "Analysis of the electromagnetic acoustic noise and vibrations of a high-speed brushless DC motor," in *Eighth IET International Conference on Power Electronics, Machine and Drives (PEMD),* pp.1-10, Apr. 2016.

[5] S. Lin, C. Bi, and Q. Jiang, "Analysis of acoustic noise sources of BLDC and ADB spindle motors operating at BLDC mode," in *Fourth IET International Conference on Power Electronics, Machine and Drives (PEMD),* pp. 315-319, Apr. 2008.

[6] A. Saxena and B. G. Fernandes, "Noise and cogging torque reduction in brushless DC ceiling fan," in *18th International Conference on Electrical Machines and Systems (ICEMS),* pp. 1334-1338, Oct. 2015.

[7] D. Torregrossa, A. Khoobroo, and B. Fahimi, "Prediction of acoustic noise and torque pulsation in PM synchronous machines with static eccentricity and partial demagnetization using field reconstruction method," *IEEE Trans. Ind. Electron.,* Vol. 59, No. 2, pp. 934-944, May 2011.

[8] R. Sathya, A. Sivaprakasam, and T. Manigandan, "Analysis and experimental investigation to mitigate mechanical vibration and acoustic noise in direct torque controller fed PMSM," *International Journal of Research in Engineering and Technology,* Vol. 3, No. 7, pp. 80-88, May 2014.

[9] J. H. Leong and Z. Q. Zhu, "Acoustic noise and vibration of direct-torque-controlled permanent magnet brushless DC drives," in *6th IET International Conference on Power Electronics, Machines and Drives (PEMD),* pp. 1-6, Mar. 2012.

[10] S. Sung, G. Jang, K. Kang, and J. Song, "Effect of additional harmonics of driving current on torque ripple and unbalanced magnetic force in HDD spindle motors with stator and rotor eccentricity," *Microsystem Technologies,* Vol. 21, No. 12, pp. 2669-2678, Dec. 2015.

[11] S. Lin, C. Bi, and Q. Jiang, "Analysis of acoustic noise sources of FDB and ADB spindle motors operating at BLDC mode," in *4th IET conference on Power Electronics, Machines and Drives (PEMD),* pp. 315-319, Apr. 2008.

[12] S. K. Chang and J.-S. Seol, "New cogging-torque reduction method for brushless permanent-magnet motors," *IEEE Trans. Magn.,* Vol. 39, No. 6, pp. 3503-3506, Nov. 2003.

[13] Y.-K. Lin and Y.-S. Lai, "Pulsewidth modulation technique for BLDCM drives to reduce commutation torque ripple without calculation of commutation time," *IEEE Trans. Ind. Appl.,* Vol. 47, No. 4, pp. 1786-1793, Jul./Aug. 2011.

[14] J. Shi and T.-C. Li, "New method to eliminate commutation torque ripple of brushless DC motor with minimum commutation time," *IEEE Trans. Ind. Electron.*, Vol. 60, No. 6, pp. 2139-2146, Jun. 2013.

[15] J. Fang, H. Li, and B. Han, "Torque ripple reduction in BLDC torque motor with nonideal Back EMF," *IEEE Trans. Power Electron.,* Vol. 27, No. 11, pp. 4630-4637, Nov. 2011.

[16] S. B. Ozturk and H. A. Toliyat, "Direct torque and indirect flux control of brushless DC Motor," *IEEE/ASME Trans. Mechatronics*, Vol. 16, No. 2, pp. 351-360, Apr. 2011.

[17] P Kampmann, and F Kirchner, "Integration of fiber-optic sensor arrays into a multi-modal tactile sensor processing system for robotic end-effectors," *sensors*, Vol. 14, No. 4, pp. 6854-6876, 2014.

[18] Z. Hao, G. Chen, and X. Zhang, "A differential electromagnetic induction torque sensor and its finite element analysis," *Review of Scientific Instruments*, Vol. 86, No. 5, pp. 333-346, May 2015.

[19] X. Ji, Y. Fan, H. Qi, J. Chen, T. Han, and P. Cai, "A wireless demodulation system for passive surface acoustic wave torque sensor," *Review of Scientific Instruments*, Vol. 85, No. 12, pp. 125001-125008, Dec. 2014.

[20] K. Xia, J. Lu, C. Bi, Y. Tuan, and B. Dong, "Dynamic commutation torque-ripple reduction for brushless dc motor based on quasi-Z-source Net," *IET Electric Power Applications*, Vol. 10, No. 9, pp. 819-826, Nov. 2016.

[21] T. Sun, J.-M. Kim, G.-H. Lee, J.-P. Hong, and M.-R. Choi, "Effect of pole and slot combination on noise and vibration in permanent magnet synchronous motor," *IEEE Trans. Magn.*, Vol. 47, No. 5, pp. 1038-1041, May 2011.

[22] R. Islam and I. Husain, "Analytical model for predicting noise and vibration in permanent-magnet synchronous motors," *IEEE Trans. Ind. Appl.*, Vol. 46, No. 6, pp. 2346-2354, Nov./Dec. 2010.

[23] K. Xia, J. Lu, B. Dong, and C. Bi. "Analysis of acoustic noise from electromagnetic torque ripple for brushless DC motor," in *Asia-Pacific Magnetic Recording Conference Digest (APMRC),* pp.1-2, Jul. 2016.

[24] J. Le Besnerais, Q. Souron, and E. Devillers. "Analysis of the electromagnetic noise and vibrations of a high-speed brushless DC motor," in *8th IET International Conference on Power Electronics, Machines and Drives (PEMD),* pp. 1-10, Apr. 2016.

[25] J. Li, Y. Xu, and J. Zou, "A study on the reduction of vibration and acoustic noise for brushless DC motor," in *International Conference on Electrical Machines and Systems (ICEMS),* pp. 561-563, Oct. 2008.

Kun Xia was born in China, in 1980. He received his B.S. degree in Industrial Automation and his Ph.D. degree in Power Electronics and Power Drives from the Hefei University of Technology (HFUT), Hefei, China, in 2002 and 2007, respectively. He was a Visiting Scholar in the Electrical and Computer Engineering Department of the National University of Singapore, Singapore, in 2015. From 2007 to 2011, he was a Lecturer in the University of Shanghai for Science and Technology (USST), Shanghai, China, where he has been an Associate Professor and a Department Head in the Department of Electrical Engineering, since 2011. His current research interests include motors and motor control.

Zhengrong Li was born in China, in 1992. He received his B.S. degree from the University of Shanghai for Science and Technology (USST), Shanghai, China, and the Liverpool John Moores University, Liverpool, ENG, UK, in 2015. He is presently a Postgraduate at USST. His current research interests include motors, motor control and inverter topologies.

Jing Lu was born in China, in 1993. She received her B.S. degree from the University of Shanghai for Science and Technology (USST), Shanghai, China, in 2014. She is presently a Postgraduate at USST. Her current research interests include motors, motor control and digital circuits.

Bin Dong was born in China, in 1993. He received his B.S. degree from University of Shanghai for Science and Technology (USST), Shanghai, China, in 2014. He is presently a Postgraduate at USST. His current research interests include motors, motor control and high-voltage circuits.

Chao Bi was born in China, in 1958. He received his B.S. degree in Electrical Engineering from the Hefei University of Technology (HFUT), Hefei, China; his M.S. degree in Electrical Engineering from Xi'an Jiaotong University, Xi'an, China; and his Ph.D. degree in Electrical Engineering from the National University of Singapore, Singapore, in 1982, 1984 and 1994, respectively. From 1984 to 1990, he was a Lecturer at Southeast University (SEU), Nanjing, China. From 1994 to 1996, he was a Senior Engineer in Western Digital (S) Pte. Ltd., Singapore. From 1996 to 2003, he was a Principle Engineer, from 2003 to 2007, he was a Research Scientist, and from 2007 to 2014, he was a Senior Scientist in the Data Storage Institute (DSI), Agency for Science, Technology and Research (A*STAR), Singapore. Since 2005, he has been an Associate Professor in the Department of Electrical and Computer Engineering of the National University of Singapore. Since 2016, he has been a Professor in the University of Shanghai for Science and Technology (USST), Shanghai, China. He is the author of one book and more than 120 articles. He also has 8 inventions to his credit. Prof. Bi was a recipient of the National Technology Award of Singapore in 2006. His current research interest includes motor design, MEMS, and actuator design and optimization.